

# HDRUNet: Single Image HDR Reconstruction with Denoising and Dequantization

Xiangyu Chen<sup>1</sup> Yihao Liu<sup>1,2</sup> Zhengwen Zhang<sup>1</sup> Yu Qiao<sup>1,3</sup> Chao Dong<sup>1,4\*</sup>

<sup>1</sup>Key Laboratory of Human-Machine Intelligence-Synergy Systems,

Shenzhen Institutes of Advanced Technology, Chinese Academy of Sciences

<sup>2</sup>University of Chinese Academy of Sciences <sup>3</sup>Shanghai AI Lab, Shanghai, China

<sup>4</sup>SIAT Branch, Shenzhen Institute of Artificial Intelligence and Robotics for Society

{chxy95, zhengwen.zhang02}@gmail.com liuyihao14@mails.ucas.ac.cn {yu.qiao, chao.dong}@siat.ac.cn

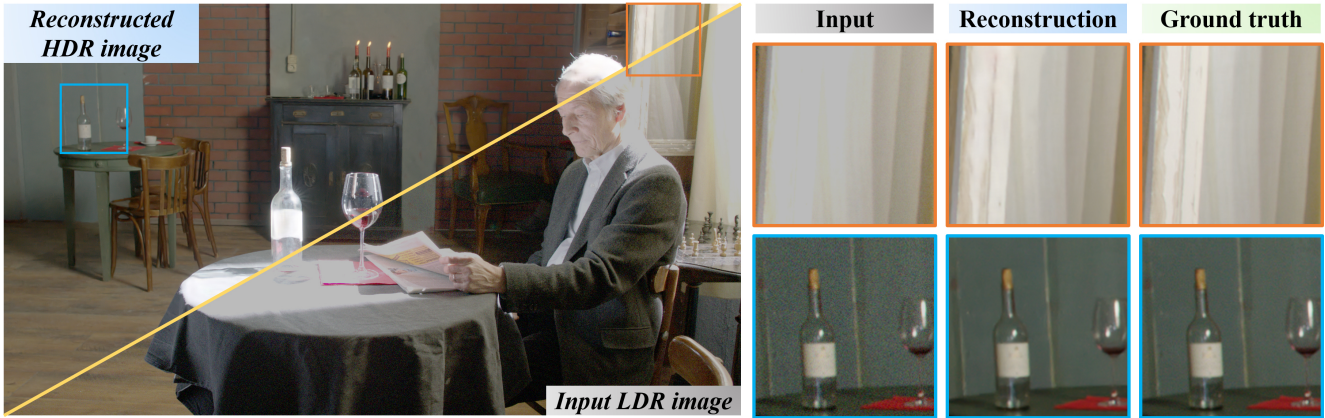


Figure 1. HDR reconstruction with denoising and dequantization from a single LDR image. We propose a novel learning based method for single image HDR reconstruction with denoising and dequantization. The proposed method consists of a spatially dynamic encoder-decoder network and a new  $\text{Tanh}_L L_1$  loss function. The visual comparison shows that our method reconstructs information in over-exposed regions and also reduces the noise and quantization loss in well-exposed regions. All the images have been  $\mu$ -law tone-mapped for display. We slightly increase the contrast of patches in the bottom row for clearer visualization. **Please zoom in for best view.**

## Abstract

Most consumer-grade digital cameras can only capture a limited range of luminance in real-world scenes due to sensor constraints. Besides, noise and quantization errors are often introduced in the imaging process. In order to obtain high dynamic range (HDR) images with excellent visual quality, the most common solution is to combine multiple images with different exposures. However, it is not always feasible to obtain multiple images of the same scene and most HDR reconstruction methods ignore the noise and quantization loss. In this work, we propose a novel learning-based approach using a spatially dynamic encoder-decoder network, HDRUNet, to learn an end-to-end mapping for single image HDR reconstruction with denoising and dequantization. The network consists of a UNet-style base network to make full use of the hierarchical multi-scale information, a condition network to

perform pattern-specific modulation and a weighting network for selectively retaining information. Moreover, we propose a  $\text{Tanh}_L L_1$  loss function to balance the impact of over-exposed values and well-exposed values on the network learning. Our method achieves the state-of-the-art performance in quantitative comparisons and visual quality. The proposed HDRUNet model won the second place in the single frame track of NITRE2021 High Dynamic Range Challenge. The code is available at <https://github.com/chxy95/HDRUNet>.

## 1. Introduction

High dynamic range (HDR) images are capable of recording a more realistic appearance of the scene, which can significantly improve the viewing experience. However, limited by the sensor, most consumer-grade digital cameras can only capture a limited range of luminance. In addition, noise and quantization errors are often introduced in

the imaging processing. The most commonly used method to generate an HDR image is to merge a set of LDR images captured with different exposures [9]. However, these approaches have to deal with the object motion among different LDR images [51, 26, 39, 23], and multiple images captured at the same scene are not always feasible. Besides, most HDR reconstruction methods only focus on dynamic range expansion [13, 44] and ignore the noise and quantization loss in the well-exposed regions.

Single image HDR reconstruction with denoising and dequantization is a challenging problem. First, it is hard to recover the missing details in the under-/over-exposed regions from a single LDR input due to severe information loss. Second, dealing with the problem of joint HDR reconstruction, denoising and dequantization is a challenge for the network design and training. Some traditional single image HDR reconstruction approaches directly improve the brightness or enhance the contrast of the input [37, 38, 1]. A number of techniques utilize image local heuristics to expand the dynamic range [4, 30]. Most recent data-driven single image HDR reconstruction methods deal with the problem by recovering the over-exposed regions [13]. Note that these methods are all proposed to predict the linear HDR values in luminance domain and do not explicitly perform denoising. There are also several methods that have been proposed recently, aiming at predicting the non-linear HDR values in display format under the HDR standard [27, 28]. They also do not consider the denoising issues.

In this work, we aim to predict a non-linear 16-bit HDR image after gamma correction from a single 8-bit LDR noisy image. We propose a spatially dynamic encoder-decoder network, called HDRUNet, to deal with restoration details in under-/over-exposed regions along with denoising and dequantization for the whole image. We design our approach based on two observations. First, noise and quantization errors certainly exist in LDR images in comparison with their HDR ground truths, and the patterns in over-exposed regions are obviously different from those in well-exposed regions. Second, distributions of noise are spatially variant, which are not uniform like Gaussian white noise. In order to address these issues, we first design a network consisting of three parts, including a UNet-like base network that can utilize multi-scale information, a condition network that performs spatially dynamic modulation for different patterns, and a weighting network for adaptively retaining information of the input. Besides, we propose a new  $Tanh\_L_1$  loss function that normalizes values into  $[0, 1]$  to balance the impact of high luminance values and the other values during training, in order to prevent the network from only focusing on high luminance values.

Our contributions are three-fold:

- We propose a new deep network to reconstruct a high quality HDR image with denoising and dequantization

from a single LDR image.

- We introduce a  $Tanh\_L_1$  loss for the task. Compared to the other commonly used losses of image restoration, this loss can lead to better quantitative performance and visual quality.
- Experiments show that our method outperforms the state-of-the-art methods both quantitatively and qualitatively, and we won the second place in the single frame track of NTIRE2021 HDR Challenge [40].

## 2. Related Work

### 2.1. HDR Reconstruction

The task of image HDR reconstruction, which is also known as inverse tone mapping [4], has been extensively studied in the previous decades. The most common technique is to fuse a stack of bracketed exposure LDR images [9]. There are also recent methods applying CNNs to fuse multiple LDR images [51, 26, 14]. In this paper, we focus on reconstructing HDR image from a single LDR image.

Traditional single image HDR reconstruction methods exploit internal image characteristics to predict the luminance of the scene. For example, [1, 3, 4, 5] estimate the density of light sources to expand the dynamic range and [25, 30] apply cross-bilateral filter to enhance the input LDR images. There are also several approaches [37, 38] using global operator for approximating tone expansion to improve the visual quality.

Recently CNNs have also shown great performance for image restoration and enhancement tasks such as image super-resolution [11], compression artifact reduction [10], denoising [53], photo retouching [19] and inpainting [52], etc. Several methods have been developed to learn a direct LDR-to-HDR mapping. Eilertsen et al. [13] propose HDRCNN to recover missing details in the over-exposed regions and Santos et al. [44] improve the method by adding masked features and perceptual loss. However, their methods ignore the quantization artifacts and noise in the well-exposed areas. SingleHDR [34] learns LDR-to-HDR mapping by reversing the camera pipeline. These approaches aim at predicting the linear HDR luminance. Kim et al. [27] propose Deep SR-ITM to solve the problem of joint super-resolution and inverse tone-mapping, while they aim to predict HDR pixel values in display format under HDR standard involving wide color gamut and HDR transfer function. In this work, we focus on the problem of single image HDR reconstruction with denoising and dequantization.

### 2.2. Denoising

Image denoising is a classic topic in the field of low level vision. Traditional methods use various models to model the image prior to achieve denoising, such as [6, 35, 12, 16, 50]. These prior-based methods are generally time-

consuming and involve manually chosen parameters. Recently, there have been several attempts to perform denoising by CNNs [53, 42, 36]. However, these methods are designed for Gaussian white noise which usually generalize poorly to real-world noisy images [41]. For addressing this issue, several approaches are proposed by taking noise level prior as network input to handle different noise levels and spatially variant noise [54, 18, 17]. In this work, we add a spatially dynamic modulation module to perform denoising inside along with HDR reconstruction.

### 2.3. Dequantization

Quantization errors are inevitably occurred in the imaging process. It is reflected in the image as scattered noise and artifacts (e.g. contouring or banding artifacts) in regions with smooth gradient changes. Previous works on bit-depth expansion smooth image by applying the spatially adaptive filter [8] or selective average filter [47], or even directly adding noise to alleviate the artifacts [7]. Learning-based methods [22, 32, 55, 43] have been proposed recently and they usually focus on restoration from lower bit-depth input to the 8-bit image. In this work, we aiming at recovering a 16-bit HDR image from an 8-bit LDR image.

## 3. Methodology

### 3.1. Observations

The problem of image HDR reconstruction is often accompanied with denoising and dequantization. To illustrate this point, we visualize the gradient map of an LDR image and the corresponding HDR image by Scharr operator [45] as shown in Figure 2. Compared with the HDR image, gradients are less visible in highlight areas of the LDR image, due to the dynamic range compression and quantization. In the well-exposed areas, gradients of noises are clear in the LDR and HDR images, indicating that noise exists in both images. Nevertheless, patterns of noise are markedly different between LDR and HDR images due to different noise levels. In addition, unlike Gaussian white noise that is uniformly distributed throughout the whole image, distribution of noises in these images are not uniform. Therefore, the pattern difference does not only exist between the highlight and non-highlight areas, but also in different positions of well-exposed regions. This inspires us to design a spatial-variant modulation module for the network.

### 3.2. Network Structure

Based on the aforementioned observation, we design a UNet-like network with spatial modulation for the single image HDR reconstruction. The overall architecture of the proposed method is depicted in Figure 3, which consists of three main components – a base network, a condition network and a weighting network.

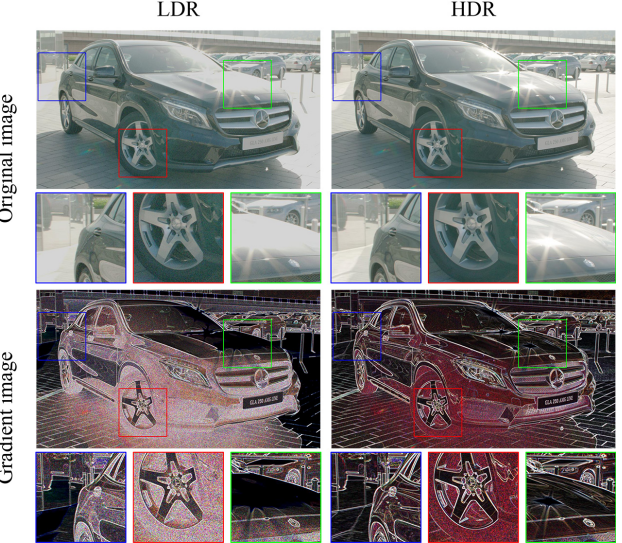


Figure 2. Gradient maps calculated by Scharr operator [45] of the LDR and HDR image. Note that the HDR image is not noise-free. It can be observed that gradients of LDR and the corresponding HDR image are obviously different both in over-exposed regions and well-exposed regions.

**Base Network.** The base network utilizes a UNet-like structure, which takes the 8-bit noisy LDR image as input and reconstructs the 16-bit HDR image. The predicted HDR images are supposed to contain more details in under-/over-exposed areas with little noise. Many image reconstruction algorithms [13, 34] have proven the effectiveness of UNet-like structure, which can make full use of the hierarchical multi-scale information from low-level features to high-level features. We adopt similar concept for this task. The encoder is devised to map the LDR image to high-dimensional representations, and the decoder is trained to reconstruct the HDR image from the encoded representations. To achieve better reconstruction performance, skip connections are added between the encoder and decoder. In the task of HDR reconstruction, the encoder and decoder work in 8-bit and 16-bit, respectively. To ease the training procedure and maximize the information flow, several residual blocks are utilized in the base network.

**Condition Network.** The key to reconstruct HDR images is to recover the missing details in under-/over-exposed regions of the input LDR image. Different areas in one image have different exposures and brightness. Further, various images also have different holistic brightness and contrast information. Hence, it is necessary to deal with input images with location-specific and image-specific operations. Besides, non-uniformly distributed noise also requires the network to process various patterns well. However, conventional convolutional neural networks are spatially variant, where the same filter weights are applied across all images and local regions. Thus, inspired by

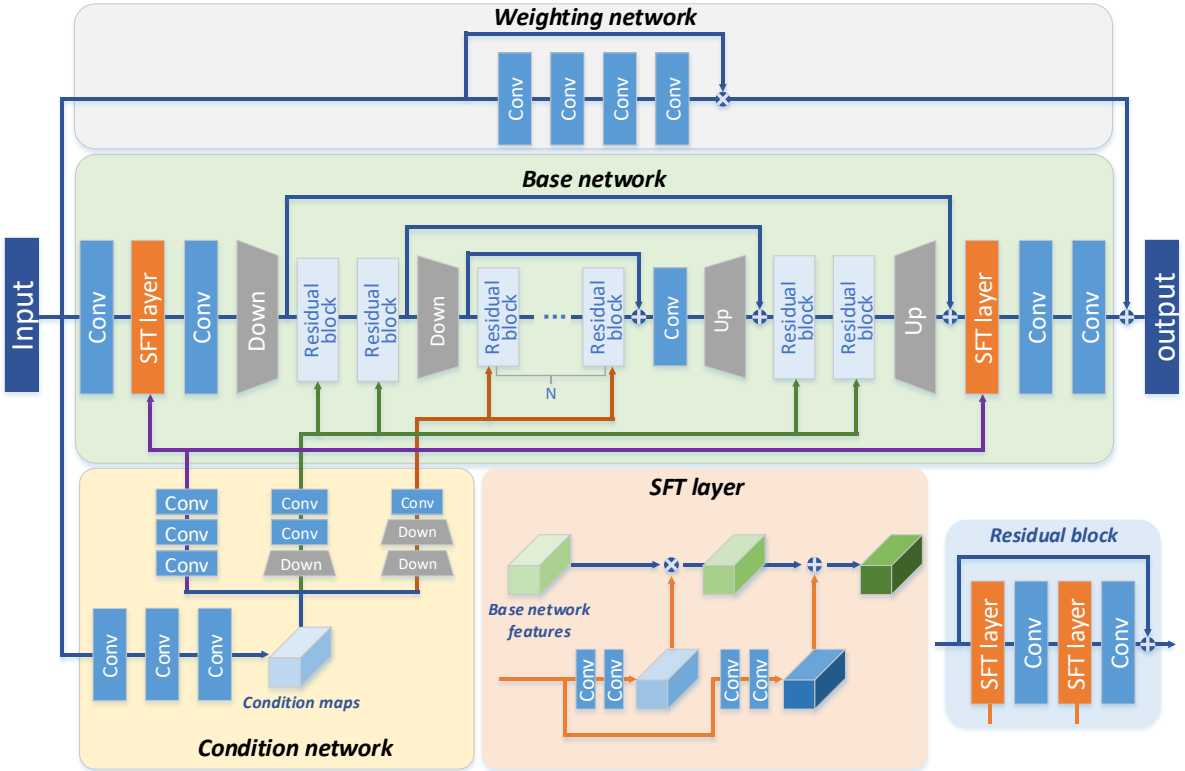


Figure 3. Network structure of our HDRUNet with a base network, a condition network and a weighting network. The three modules all take the LDR image as input. Particularly, the condition network predicts condition maps that afterwards utilized to modulate the intermediate features in the base network.

[49, 33], we introduce a condition network with spatial feature transform (SFT) [49] to provide spatially variant manipulations. Specifically, the condition network accepts the input LDR image and predicts the corresponding conditional maps that are afterwards used to modulate the intermediate features in the base network. The structure of the condition network and the mechanism of SFT layer are portrayed in Figure 3.

$$SFT(x) = \alpha \odot x + \beta, \quad (1)$$

where  $\odot$  denotes the element-wise multiplication.  $x \in \mathbb{R}^{C \times H \times W}$  is the intermediate features to be modulated.  $\alpha \in \mathbb{R}^{C \times H \times W}$  and  $\beta \in \mathbb{R}^{C \times H \times W}$  are two modulation coefficient maps predicted by the condition network. By leveraging such modulation strategy, our method can achieve location and image specific manipulation according to different inputs. Experiments have demonstrated the effectiveness of such feature modulation for HDR reconstruction with denoising and dequantization.

**Weighting Network.** The biggest challenge of HDR reconstruction is to restore fine details in under-/over-exposed regions, while most of the well-exposed contents can be of less contribution to the learning procedure. To this end, we propose a weighting estimation network to forecast a soft

weighting map  $W$  on the well-exposed regions to be retained. Thereupon, the whole network will pay more attention to reconstruct the details of over-exposed areas.

$$\hat{Y} = W \odot I + \mathcal{G}(I), \quad (2)$$

where  $I$  is the input LDR image,  $\hat{Y}$  is the final reconstructed HDR image, and  $\mathcal{G}(I)$  is the output of the base network.

### 3.3. Loss Function

In real-world image HDR reconstruction, it is necessary to consider not only the restoration of the dynamic range, but also the reduction of noise and quantization artifacts. However, loss functions that are commonly used in previous works of image restoration, such as  $L_1$  and  $L_2$  loss, are not applicable to simultaneously deal with these aforementioned problems. A loss function formulated directly on HDR values will make the network focus on high luminance values and underestimate the impact in lower luminance values, resulting in worse quantitative performance and visual quality. The experimental results can be found in Section 4.2. Therefore, we propose a specially designed  $Tanh-L_1$  loss for the task, which is formulated as:

$$Tanh\_L_1(\hat{Y}, H) = \left| \text{Tanh}(\hat{Y}) - \text{Tanh}(H) \right|, \quad (3)$$

where  $\hat{Y}$  and  $H$  represent the predicted HDR image and the corresponding ground truth image, respectively.

## 4. Experiments

### 4.1. Experimental Setup

**Dataset.** Previous studies [14, 13, 34, 27] have adopted different datasets on the task of image HDR reconstruction for training and evaluation. In this paper, we use the dataset proposed by NITRE 2021 HDR Challenge [40]. As depicted in this challenge, the dataset is a subset of images selected from the HdM HDR dataset [15], where the HDR images are captured by two Alexa Arri cameras with a mirror rig and the corresponding LDR images are generated by applying a degradation model (e.g., exposure gain, noise addition and quantization, clipping). In this dataset, there are 1494 LDR/HDR pairs for training, 60 images for validation and 201 images for testing. Note that the LDR/HDR pairs are aligned both in time axis and exposure level and stored after gamma correction (i.e., they are non-linear images). Since the ground truths of the validation and testing set are not available, we conduct the experiments only based on the training set. The training set is composed of 1494 consecutive frames in 26 long takes. We randomly select 3 frames in every long take, a total of 78 frames, as the verification set, and the rest 1416 frames are used for training.

**Evaluation Metrics.** In the challenge, standard PSNR directly computed in the output images (normalized to the peak value of the ground-truth HDR image) and PSNR computed in the  $\mu$ -law tone-mapped images (normalized to the 99 percentile of the ground-truth image and bounded by a Tanh function to avoid excessive brightness compression) are used as the evaluation metrics. We represent these two metrics as PSNR-L and PSNR- $\mu$ , respectively. It can be seen that PSNR-L and PSNR- $\mu$  have different tendencies for evaluating image quality. For s-PSNR, the accuracy of highlight values is the most important influential factor. However, these values are often severely compressed by tone mapping for visualization. While PSNR- $\mu$  directly measures the tone-mapped values that can directly reflect the visual similarity of the result and the ground truth. Therefore, the main measure in quantitative comparisons is PSNR- $\mu$  both in the challenge and in this paper.

**Implementation Details.** In the following experiments, the number of residual blocks  $N$  is set to 8. Convolution filters with stride of 2 are used for down-sampling and pixel shuffle [46] is utilized for up-sampling. Before training, we pre-process the data by cropping images into  $480 \times 480$  with step of 240. During training, the mini-batch size is set to 16 and the number of training iterations is set to  $1 \times 10^6$ . Adam [29] optimizer and Kaiming-initialization [20] are adopted for training. The initial learning rate is set to  $2 \times 10^{-4}$  and decayed by a factor of 2 after every  $2 \times 10^5$  iterations. All

models are built on the PyTorch framework and trained with NVIDIA 2080Ti GPU. When the patch size of input is set to  $256 \times 256$ , the total training time is about 5 days.

### 4.2. Ablation Study

In this section, we conduct ablation study to further investigate the different settings, including the training patch size, loss functions, key modules and modulation strategies.

**Training Patch Size.** In practice, we find that the training patch size has an important influence on this task. In general, small patch size (e.g.,  $32 \times 32$  or  $64 \times 64$ ) is usually adopted during training in super-resolution networks [11, 48]. However, HDR reconstruction is more than a simple local process. It involves more global and holistic manipulations, since different regions in LDR image require different treatments. Besides, due to severe information loss in over-exposed regions, we believe that restoration of the details needs a large receptive field in these areas. As shown in Table 1, with the increase of patch size, the quantitative performance is gradually improved. To consider both performance and computational cost, we select  $256 \times 256$  as the recommended patch size.

Patch size	PSNR-L (dB)	PSNR- $\mu$ (dB)
48	39.82	33.43
96	40.60	33.78
160	41.13	33.94
256	41.61	34.02

Table 1. Influence of training patch size.

**Loss Function.** In Section 3.3, we introduce a  $Tanh\_L_1$  loss for HDR reconstruction with denoising and dequantization. To accelerate the training process, we fix the patch size to  $160 \times 160$ . To validate the effectiveness of our proposed loss function, we conduct experiments with various loss functions and make quantitative and qualitative comparisons. The quantitative results are shown in Table 2, from which we can draw the following observations: 1) Compared with  $L_2$  loss,  $L_1$  loss can obtain better quantitative performance with higher PSNR-L and PSNR- $\mu$  values. 2) By introducing  $Tanh$  operation, the PSNR- $\mu$  can be further improved at the cost of PSNR-L. To be specific, using  $Tanh\_L_1$  loss improves PSNR- $\mu$  by 0.35 dB. This is because when  $L_1$  or  $L_2$  loss function is used directly, the training loss of the high brightness value has larger weight. In this case, the network mainly focuses on the highlight areas, leading to higher PSNR-L. However, as depicted in Section 4.1, PSNR- $\mu$  can better reflect the visual similarity of the output with the ground truth. Since the PSNR- $\mu$  is also the main reference evaluation metric in the challenge, we adopt  $Tanh\_L_1$  as the loss function.

Loss	PSNR-L (dB)	PSNR- $\mu$ (dB)
$L_2$	43.91	31.80
$L_1$	44.10	33.59
$Tanh-L_2$	40.02	33.92
$Tanh-L_1$	41.13	33.94

Table 2. Quantitative comparison of different loss functions.

Moreover, the loss function also has a significant impact on the visual results. The visual comparison of these loss functions are shown in Figure 4. We can see that results generated by using  $L_1$  or  $L_2$  loss function perform badly for denoising in well-exposed regions. In contrast,  $Tanh-L_1$  loss achieves the best visual quality.

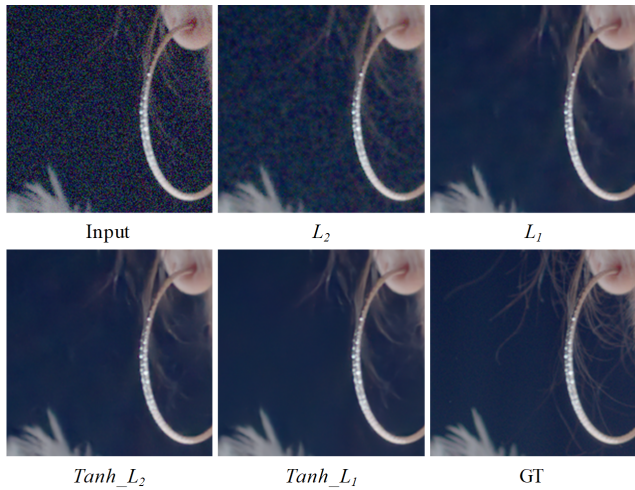


Figure 4. Visual comparison of different loss functions. It can be obviously observed that  $L_1$  or  $L_2$  loss perform badly for denoising, and our  $Tanh-L_1$  loss achieves the best visual quality.

**Effectiveness of Key Modules.** In this section, we demonstrate the effectiveness of each proposed component. The experimental results are shown in Table 3. Note that we set patch size of  $160 \times 160$  for fast training. If we only adopt a sole UNet-like base network, the PSNR-L and PSNR- $\mu$  are 40.77 dB and 33.85 dB, respectively. By adopting the weighting network branch, the performance is slightly improved. If we combine the base network and the condition network together, the PSNR-L and PSNR- $\mu$  are improved by 0.27 dB and 0.06 dB. With all three key modules equipped, our full model can further achieve higher quantitative results with PSNR-L of 41.13 dB and PSNR- $\mu$  of 33.94 dB. The results clearly validate the effectiveness of the proposed key modules.

**Exploration on Modulation Strategy.** Feature modulation has proven to be an effective way to tackle image-specific and location-specific tasks, such as photo retouch-

Network Structure	Base Network			
	Condition Network	X	X	✓
Weighting Network	X	✓	X	✓
PSNR-L (dB)	40.77	40.85	41.04	41.13
PSNR- $\mu$ (dB)	33.85	33.90	33.91	33.94

Table 3. Effectiveness of each proposed component.

ing [19], image restoration [18, 17], image super-resolution [49], as well as HDR reconstruction [27]. In this paper, we adopt SFT to provide spatially variant manipulations. We also compare other feature modulation variants. In our condition network, the size of the predicted condition maps is  $C \times H \times W$ , thus, every unit of the feature maps in the based network will be modulated. The condition maps can also be of size  $1 \times H \times W$ , in which case the modulation parameters are spatial-variant but shared across channels. In contrast, the modulation in CResMD [17] is global channel-wise without considering spatial information.

Modulation strategy	PSNR-L (dB)	PSNR- $\mu$ (dB)
None	40.77	33.85
CResMD ( $C \times 1 \times 1$ )	39.84	33.65
SFT ( $1 \times H \times W$ )	40.65	33.82
SFT ( $C \times H \times W$ )	41.04	33.91

Table 4. Comparison of different modulation strategies.

The comparison results of these modulation strategies are listed in Table 4. Note that, to directly illustrate the differences among various modulation methods, we eliminate the weighting network in the experiments. From the results, it can be observed that global channel-wise modulation has little effect on HDR reconstruction, since it cannot provide any spatially variant manipulation. By introducing SFT, the performance is greatly improved, which validate our comments that different areas in LDR image should be handled differently. Moreover, spatial modulation with  $C \times H \times W$  is superior to that with  $1 \times H \times W$ , since it cannot only involve spatial-wise but also channel-wise manipulations.

### 4.3. Comparison with State-of-the-art Methods

We compare our HDRUNet with several state-of-the-art methods on image HDR reconstruction, including LandisEO [31], HuoEO [24], HDRCNN [13], SingleHDR [34], Deep SR-ITM [27] and a ResNet-style [21] network. However, most of these methods utilize different datasets that contain many specific operations for the data to be processed. We slightly modify these algorithms or add post-

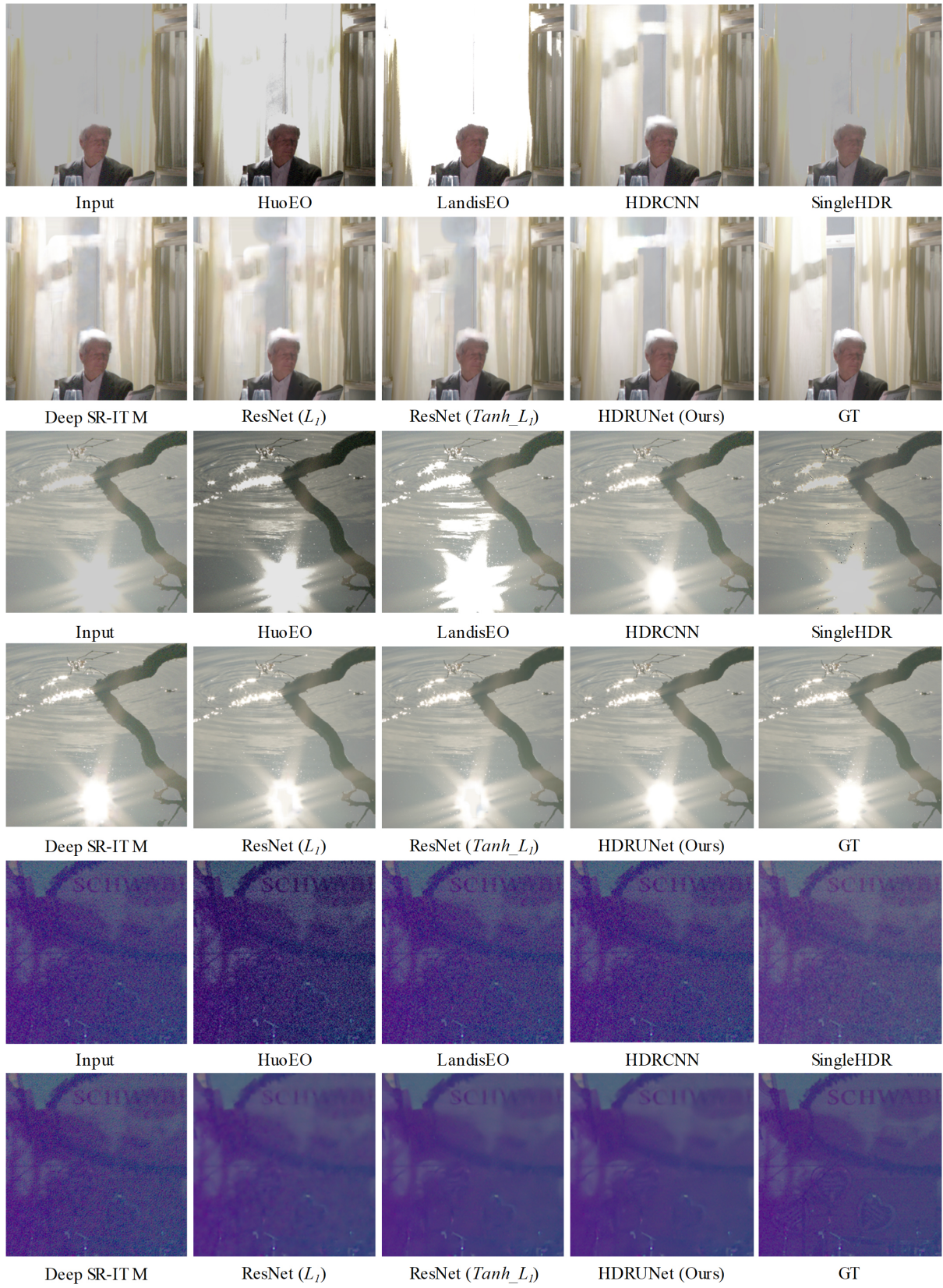


Figure 5. Qualitative comparison with other methods.

processing for this dataset. For LandisEO and HuoEO, we use the implementations in HDR Toolbox [2] and set the gamma as 2.24. Besides, we implement gamma correction on the results because these are linear HDR values. For HDRCNN, we retrain them on the same dataset as our method. We use a convolution filter with stride of 2 for down-sampling to match the size of input and output for Deep SR-ITM. Since SingleHDR is only suitable for restoring the linear HDR value in luminance domain, we directly test the pretrained model on our dataset and implement post-process as LandisEO and HuoEO. We also train a ResNet-style model that is commonly used in image restoration and utilize both  $L_1$  loss and the proposed  $\text{Tanh}_L L_1$  loss.

Method	PSNR-L (dB)	PSNR- $\mu$ (dB)
LandisEO	17.88	23.30
HuoEO	32.40	17.35
SingleHDR	32.32	19.54
HDRCNN	39.47	26.05
Deep SR-ITM	43.29	26.25
ResNet ( $L_1$ )	41.92	33.24
ResNet ( $\text{Tanh}_L L_1$ )	39.82	33.67
HDRUNet (Ours)	41.61	34.02

Table 5. Quantitative comparison with other methods.

**Quantitative Comparison.** We provide the quantitative results in Table 5. As described in Section 4.1, PSNR-L and PSNR- $\mu$  have different tendencies for evaluating image quality. PSNR-L is used to measure the accuracy of the high luminance values, while PSNR- $\mu$  reflects the visual similarity between predicted HDR image and the ground truth. For LandisEO, HuoEO and SingleHDR, these methods predict linear HDR values. Although we perform gamma correction on the results, it is still very difficult to align the exposure completely. Thus the results generated by these methods perform badly in such reference-based metrics. HDRCNN and Deep SR-ITM learn direct mapping from LDR to HDR, while HDRCNN only processes values in over-exposed regions. Deep SR-ITM uses a big network with  $L_2$  loss function, which brings higher PSNR-L and lower PSNR- $\mu$ . It can be seen that our method achieves the best quantitative performance in PSNR- $\mu$  and far above average performance in PSNR-L.

**Qualitative Comparison.** We provide the qualitative comparison in Figure 5. Our method can not only restore fine details in highlight regions but also greatly reduce noise in lower luminance area. On the contrary, although the other methods improve the brightness of the highlight areas, they hardly recover details in these areas and some of them introduce additional artifacts. LandisEO uses a global oper-

ator to increase the brightness in over-exposed regions but can not generate details. HuoEO and ResNet generate some details but introduce additional artifacts at the same time. Additionally, these methods can not perform denoising and dequantization well. Noise can be clearly observed in the well-exposed regions. In comparison of these approaches, results of our method achieve the best visual quality.

#### 4.4. Results of NTIRE2021 HDR Challenge

We participated in the NTIRE2021 HDR Challenge [40] and won the second place in the single frame track. The results are shown in Table 6. Without using ensemble approaches, our method obtains similar PSNR- $\mu$  score as the first place, only about 0.07 dB apart. Besides, the running speed of ours is more than 116 times that of the first place.

Team	PSNR- $\mu$	PSNR-L	Runtime (s)	Ensemble
NOAHTCV	34.804	32.867	61.52	✓
XPixel (ours)	34.736	32.285	0.53	-
BOE-IOT-AIBD	34.414	33.490	5.00	-
CET CVLab	33.874	32.06	0.20	✓
CVRG	32.778	31.021	1.10	-

Table 6. Results of the top5 methods in the challenge.

## 5. Conclusion

In this paper, we propose a spatially dynamic encoder-decoder network, HDRUNet, with a novel  $\text{Tanh}_L L_1$  loss function to solve the single image HDR reconstruction problem. Our method won the second place in the single frame track of NTIRE2021 HDR Challenge. Particularly, the proposed network contains three modules which are a base network, a condition network and a weighting network. The base network can exploit multi-scale information to reconstruct HDR image. The condition network makes use of SFT layer to perform spatial-variant modulation for various patterns. The weighting network can retain useful information of the input LDR image for helping learning. Moreover, we introduce a  $\text{Tanh}_L L_1$  loss to balance the weight of learning for high luminance values and the other values. Using this function greatly facilitates learning for joint HDR reconstruction with denoising and dequantization. Overall, our methods outperforms state-of-the-art methods in quantitative and qualitative comparisons.

**Acknowledgement.** This work was supported in part by the Shanghai Committee of Science and Technology, China (Grant No. 20DZ1100800), in part by the National Natural Science Foundation of China under Grant (61906184), Science and Technology Service Network Initiative of Chinese Academy of Sciences (KJFSTSQYZX092), Shenzhen Institute of Artificial Intelligence and Robotics for Society.

## References

- [1] Ahmet Oğuz Akyüz, Roland Fleming, Bernhard E Riecke, Erik Reinhard, and Heinrich H Bülthoff. Do hdr displays support ldr content? a psychophysical evaluation. *ACM Transactions on Graphics (TOG)*, 26(3):38–es, 2007. [2](#)
- [2] Francesco Banterle, Alessandro Artusi, Kurt Debattista, and Alan Chalmers. *Advanced High Dynamic Range Imaging (2nd Edition)*. AK Peters (CRC Press), Natick, MA, USA, July 2017. [8](#)
- [3] Francesco Banterle, Kurt Debattista, Alessandro Artusi, Sumanta Pattanaik, Karol Myszkowski, Patrick Ledda, and Alan Chalmers. High dynamic range imaging and low dynamic range expansion for generating hdr content. In *Computer graphics forum*, volume 28, pages 2343–2367. Wiley Online Library, 2009. [2](#)
- [4] Francesco Banterle, Patrick Ledda, Kurt Debattista, and Alan Chalmers. Inverse tone mapping. In *Proceedings of the 4th international conference on Computer graphics and interactive techniques in Australasia and Southeast Asia*, pages 349–356, 2006. [2](#)
- [5] Francesco Banterle, Patrick Ledda, Kurt Debattista, Alan Chalmers, and Marina Bloj. A framework for inverse tone mapping. *The Visual Computer*, 23(7):467–478, 2007. [2](#)
- [6] Kostadin Dabov, Alessandro Foi, Vladimir Katkovnik, and Karen Egiazarian. Image denoising by sparse 3-d transform-domain collaborative filtering. *IEEE Transactions on image processing*, 16(8):2080–2095, 2007. [2](#)
- [7] Scott J Daly and Xiaofan Feng. Bit-depth extension using spatiotemporal microdither based on models of the equivalent input noise of the visual system. In *Color Imaging VIII: Processing, Hardcopy, and Applications*, volume 5008, pages 455–466. International Society for Optics and Photonics, 2003. [3](#)
- [8] Scott J Daly and Xiaofan Feng. Decontouring: Prevention and removal of false contour artifacts. In *Human Vision and Electronic Imaging IX*, volume 5292, pages 130–149. International Society for Optics and Photonics, 2004. [3](#)
- [9] Paul E Debevec and Jitendra Malik. Recovering high dynamic range radiance maps from photographs. In *ACM SIGGRAPH 2008 classes*, pages 1–10. 2008. [2](#)
- [10] Chao Dong, Yubin Deng, Chen Change Loy, and Xiaoou Tang. Compression artifacts reduction by a deep convolutional network. In *Proceedings of the IEEE International Conference on Computer Vision*, pages 576–584, 2015. [2](#)
- [11] Chao Dong, Chen Change Loy, Kaiming He, and Xiaoou Tang. Learning a deep convolutional network for image super-resolution. In *European conference on computer vision*, pages 184–199. Springer, 2014. [2, 5](#)
- [12] Weisheng Dong, Lei Zhang, Guangming Shi, and Xin Li. Nonlocally centralized sparse representation for image restoration. *IEEE transactions on Image Processing*, 22(4):1620–1630, 2012. [2](#)
- [13] Gabriel Eilertsen, Joel Kronander, Gyorgy Denes, Rafał K Mantiuk, and Jonas Unger. Hdr image reconstruction from a single exposure using deep cnns. *ACM transactions on graphics (TOG)*, 36(6):1–15, 2017. [2, 3, 5, 6](#)
- [14] Yuki Endo, Yoshihiro Kanamori, and Jun Mitani. Deep reverse tone mapping. *ACM Trans. Graph.*, 36(6):177–1, 2017. [2, 5](#)
- [15] Jan Froehlich, Stefan Grandineti, Bernd Eberhardt, Simon Walter, Andreas Schilling, and Harald Brendel. Creating cinematic wide gamut hdr-video for the evaluation of tone mapping operators and hdr-displays. In *Digital photography X*, volume 9023, page 90230X. International Society for Optics and Photonics, 2014. [5](#)
- [16] Shuhang Gu, Lei Zhang, Wangmeng Zuo, and Xiangchu Feng. Weighted nuclear norm minimization with application to image denoising. In *Proceedings of the IEEE conference on computer vision and pattern recognition*, pages 2862–2869, 2014. [2](#)
- [17] Jingwen He, Chao Dong, and Yu Qiao. Interactive multi-dimension modulation with dynamic controllable residual learning for image restoration. *arXiv preprint arXiv:1912.05293*, 2019. [3, 6](#)
- [18] Jingwen He, Chao Dong, and Yu Qiao. Modulating image restoration with continual levels via adaptive feature modification layers. In *Proceedings of the IEEE/CVF Conference on Computer Vision and Pattern Recognition*, pages 11056–11064, 2019. [3, 6](#)
- [19] Jingwen He, Yihao Liu, Yu Qiao, and Chao Dong. Conditional sequential modulation for efficient global image retouching. *arXiv preprint arXiv:2009.10390*, 2020. [2, 6](#)
- [20] Kaiming He, Xiangyu Zhang, Shaoqing Ren, and Jian Sun. Delving deep into rectifiers: Surpassing human-level performance on imagenet classification. In *Proceedings of the IEEE international conference on computer vision*, pages 1026–1034, 2015. [5](#)
- [21] Kaiming He, Xiangyu Zhang, Shaoqing Ren, and Jian Sun. Deep residual learning for image recognition. In *Proceedings of the IEEE conference on computer vision and pattern recognition*, pages 770–778, 2016. [6](#)
- [22] Xianxu Hou and Guoping Qiu. Image companding and inverse halftoning using deep convolutional neural networks. *arXiv preprint arXiv:1707.00116*, 2017. [3](#)
- [23] Jun Hu, Orazio Gallo, Kari Pulli, and Xiaobai Sun. Hdr deghosting: How to deal with saturation? In *Proceedings of the IEEE Conference on Computer Vision and Pattern Recognition*, pages 1163–1170, 2013. [2](#)
- [24] Yongqing Huo, Fan Yang, and Vincent Brost. Dodging and burning inspired inverse tone mapping algorithm. *Journal of Computational Information Systems*, 9(9):3461–3468, 2013. [6](#)
- [25] Yongqing Huo, Fan Yang, Le Dong, and Vincent Brost. Physiological inverse tone mapping based on retina response. *The Visual Computer*, 30(5):507–517, 2014. [2](#)
- [26] Nima Khademi Kalantari and Ravi Ramamoorthi. Deep high dynamic range imaging of dynamic scenes. *ACM Trans. Graph.*, 36(4):144–1, 2017. [2](#)
- [27] Soo Ye Kim, Jihyong Oh, and Munchurl Kim. Deep sr-itm: Joint learning of super-resolution and inverse tone-mapping for 4k uhd hdr applications. In *Proceedings of the IEEE International Conference on Computer Vision*, pages 3116–3125, 2019. [2, 5, 6](#)

- [28] Soo Ye Kim, Jihyong Oh, and Munchurl Kim. Jsi-gan: Gan-based joint super-resolution and inverse tone-mapping with pixel-wise task-specific filters for uhd hdr video. In *AAAI*, pages 11287–11295, 2020. 2
- [29] Diederik P Kingma and Jimmy Ba. Adam: A method for stochastic optimization. *arXiv preprint arXiv:1412.6980*, 2014. 5
- [30] Rafael P Kovaleski and Manuel M Oliveira. High-quality reverse tone mapping for a wide range of exposures. In *2014 27th SIBGRAPI Conference on Graphics, Patterns and Images*, pages 49–56. IEEE, 2014. 2
- [31] Hayden Landis. Production-ready global illumination. In *Siggraph 2002*, volume 5, pages 93–95, 2002. 6
- [32] Chang Liu, Xiaolin Wu, and Xiao Shu. Learning-based dequantization for image restoration against extremely poor illumination. *arXiv preprint arXiv:1803.01532*, 2018. 3
- [33] Yihao Liu, Jingwen He, Xiangyu Chen, Zhengwen Zhang, Hengyuan Zhao, Chao Dong, and Yu Qiao. Very lightweight photo retouching network with conditional sequential modulation. *arXiv preprint arXiv:2104.06279*, 2021. 4
- [34] Yu-Lun Liu, Wei-Sheng Lai, Yu-Sheng Chen, Yi-Lung Kao, Ming-Hsuan Yang, Yung-Yu Chuang, and Jia-Bin Huang. Single-image hdr reconstruction by learning to reverse the camera pipeline. In *Proceedings of the IEEE/CVF Conference on Computer Vision and Pattern Recognition*, pages 1651–1660, 2020. 2, 3, 5, 6
- [35] Julien Mairal, Francis Bach, Jean Ponce, Guillermo Sapiro, and Andrew Zisserman. Non-local sparse models for image restoration. In *2009 IEEE 12th international conference on computer vision*, pages 2272–2279. IEEE, 2009. 2
- [36] Xiao-Jiao Mao, Chunhua Shen, and Yu-Bin Yang. Image restoration using very deep convolutional encoder-decoder networks with symmetric skip connections. *arXiv preprint arXiv:1603.09056*, 2016. 3
- [37] Belen Masia, Sandra Agustin, Roland W Fleming, Olga Sorkine, and Diego Gutierrez. Evaluation of reverse tone mapping through varying exposure conditions. In *ACM SIGGRAPH Asia 2009 papers*, pages 1–8. 2009. 2
- [38] Belen Masia and Diego Gutiérrez. Dynamic range expansion based on image statistics. *Multimedia Tools and Applications*, 76, 01 2017. 2
- [39] Tae-Hyun Oh, Joon-Young Lee, Yu-Wing Tai, and In So Kweon. Robust high dynamic range imaging by rank minimization. *IEEE transactions on pattern analysis and machine intelligence*, 37(6):1219–1232, 2014. 2
- [40] Eduardo Pérez-Pellitero, Sibi Catley-Chandar, Aleš Leonardis, Radu Timofte, et al. NTIRE 2021 challenge on high dynamic range imaging: Dataset, methods and results. In *IEEE/CVF Conference on Computer Vision and Pattern Recognition Workshops*, 2021. 2, 5, 8
- [41] Tobias Plotz and Stefan Roth. Benchmarking denoising algorithms with real photographs. In *Proceedings of the IEEE conference on computer vision and pattern recognition*, pages 1586–1595, 2017. 3
- [42] Tobias Plötz and Stefan Roth. Neural nearest neighbors networks. *Advances in Neural Information Processing Systems*, 31:1087–1098, 2018. 3
- [43] Abhijith Punnappurath and Michael S Brown. A little bit more: Bitplane-wise bit-depth recovery. *arXiv preprint arXiv:2005.01091*, 2020. 3
- [44] Marcel Santana Santos, Tsang Ing Ren, and Nima Khademi Kalantari. Single image hdr reconstruction using a cnn with masked features and perceptual loss. *arXiv preprint arXiv:2005.07335*, 2020. 2
- [45] Hanno Scharr. Optimal filters for extended optical flow. In *International Workshop on Complex Motion*, pages 14–29. Springer, 2004. 3
- [46] Wenzhe Shi, Jose Caballero, Ferenc Huszár, Johannes Totz, Andrew P Aitken, Rob Bishop, Daniel Rueckert, and Zehan Wang. Real-time single image and video super-resolution using an efficient sub-pixel convolutional neural network. In *Proceedings of the IEEE conference on computer vision and pattern recognition*, pages 1874–1883, 2016. 5
- [47] Qing Song, Guan-Ming Su, and Pamela C Cosman. Hardware-efficient debanding and visual enhancement filter for inverse tone mapped high dynamic range images and videos. In *2016 IEEE International Conference on Image Processing (ICIP)*, pages 3299–3303. IEEE, 2016. 3
- [48] Xintao Wang, Kelvin CK Chan, Ke Yu, Chao Dong, and Chen Change Loy. Edvr: Video restoration with enhanced deformable convolutional networks. In *Proceedings of the IEEE/CVF Conference on Computer Vision and Pattern Recognition Workshops*, pages 0–0, 2019. 5
- [49] Xintao Wang, Ke Yu, Chao Dong, and Chen Change Loy. Recovering realistic texture in image super-resolution by deep spatial feature transform. In *Proceedings of the IEEE conference on computer vision and pattern recognition*, pages 606–615, 2018. 4, 6
- [50] Yair Weiss and William T Freeman. What makes a good model of natural images? In *2007 IEEE Conference on Computer Vision and Pattern Recognition*, pages 1–8. IEEE, 2007. 2
- [51] Shangzhe Wu, Jiarui Xu, Yu-Wing Tai, and Chi-Keung Tang. Deep high dynamic range imaging with large foreground motions. In *Proceedings of the European Conference on Computer Vision (ECCV)*, pages 117–132, 2018. 2
- [52] Raymond A Yeh, Chen Chen, Teck Yian Lim, Alexander G Schwing, Mark Hasegawa-Johnson, and Minh N Do. Semantic image inpainting with deep generative models. In *Proceedings of the IEEE conference on computer vision and pattern recognition*, pages 5485–5493, 2017. 2
- [53] Kai Zhang, Wangmeng Zuo, Yunjin Chen, Deyu Meng, and Lei Zhang. Beyond a gaussian denoiser: Residual learning of deep cnn for image denoising. *IEEE transactions on image processing*, 26(7):3142–3155, 2017. 2, 3
- [54] Kai Zhang, Wangmeng Zuo, and Lei Zhang. Ffdnet: Toward a fast and flexible solution for cnn-based image denoising. *IEEE Transactions on Image Processing*, 27(9):4608–4622, 2018. 3
- [55] Yang Zhao, Ronggang Wang, Wei Jia, Wangmeng Zuo, Xiaoping Liu, and Wen Gao. Deep reconstruction of least significant bits for bit-depth expansion. *IEEE Transactions on Image Processing*, 28(6):2847–2859, 2019. 3